

## Rotation Measure Evolution of the Repeating Fast Radio Burst Source FRB 121102

G. H. HILMARSSON,<sup>1</sup> D. MICHILLI,<sup>2,3</sup> L. G. SPITLER,<sup>1</sup> R. S. WHARTON,<sup>1</sup> P. DEMOREST,<sup>4</sup> G. DESVIGNES,<sup>1,5</sup> K. GOURDJI,<sup>6</sup>  
S. HACKSTEIN,<sup>7</sup> J. W. T. HESSELS,<sup>8,6</sup> K. NIMMO,<sup>8,6</sup> A. D. SEYMOUR,<sup>9</sup> M. KRAMER,<sup>1</sup> AND R. MCKINVEN<sup>10,11</sup>

<sup>1</sup>*Max-Planck-Institute für Radioastronomie, Auf dem Hügel 69, D-53121, Bonn, Germany*

<sup>2</sup>*Department of Physics, McGill University, 3600 rue University, Montréal, QC H3A 2T8, Canada*

<sup>3</sup>*McGill Space Institute, McGill University, 3550 rue University, Montréal, QC H3A 2A7, Canada*

<sup>4</sup>*National Radio Astronomy Observatory, Socorro, NM 87801, USA*

<sup>5</sup>*Laboratoire d'Études Spatiales et d'Instrumentation en Astrophysique, Observatoire de Paris, Université PSL  
CNRS, Sorbonne Université, Université de Paris, 5 place Jules Janssen, 92195 Meudon, France*

<sup>6</sup>*Anton Pannekoek Institute for Astronomy, University of Amsterdam, Science Park 904, 1098 XH, Amsterdam, The Netherlands*

<sup>7</sup>*Hamburger Sternwarte, University of Hamburg, Gojenbergsweg 112, D-21029, Hamburg, Germany*

<sup>8</sup>*ASTRON, Netherlands Institute for Radio Astronomy, Oude Hoogeveensedijk 4, 7991 PD, Dwingeloo, The Netherlands*

<sup>9</sup>*Green Bank Observatory, PO Box 2, WV 24944, Green Bank, USA*

<sup>10</sup>*David A. Dunlap Department of Astronomy and Astrophysics, University of Toronto, 50 St. George Street ON M5S 3H4, Toronto, Canada*

<sup>11</sup>*Dunlap Institute for Astronomy & Astrophysics, University of Toronto, 50 St. George Street, ON M5S 3H4, Toronto, Canada*

(Received June 1, 2019; Revised January 10, 2019; Accepted February 1, 2021)

### ABSTRACT

The repeating fast radio burst source FRB 121102 has been shown to have an exceptionally high and variable Faraday rotation measure (RM), which must be imparted within its host galaxy and likely by or within its local environment. In the redshifted ( $z = 0.193$ ) source reference frame, the RM decreased from  $1.46 \times 10^5 \text{ rad m}^{-2}$  to  $1.33 \times 10^5 \text{ rad m}^{-2}$  between January and August 2017, showing day-timescale variations of  $\sim 200 \text{ rad m}^{-2}$ . Here we present sixteen FRB 121102 RMs from burst detections with the Arecibo 305-m radio telescope, the Effelsberg 100-m, and the Karl G. Jansky Very Large Array, providing a record of FRB 121102's RM over a 2.5-year timespan. Our observations show a decreasing trend in RM, although the trend is not linear, dropping by an average of  $15\% \text{ year}^{-1}$  and is  $\sim 9.7 \times 10^4 \text{ rad m}^{-2}$  at the most recent epoch of August 2019. Erratic, short-term RM variations of  $\sim 10^3 \text{ rad m}^{-2} \text{ week}^{-1}$  were also observed between MJDs 58215–58247. A decades-old neutron star embedded within a still-compact supernova remnant or a neutron star near a massive black hole and its accretion torus have been proposed to explain the high RMs. We compare the observed RMs to theoretical models describing the RM evolution for FRBs originating within a supernova remnant. FRB 121102's age is unknown, and we find that the models agree for source ages of  $\sim 6 - 17$  years at the time of the first available RM measurements in 2017. We also draw comparisons to the decreasing RM of the Galactic center magnetar, PSR J1745–2900.

*Keywords:* editorials, notices — miscellaneous — catalogs — surveys

### 1. INTRODUCTION

Fast radio bursts (FRBs) are millisecond duration radio transients, whose origins are still unknown (Petroff et al. 2019). Of the roughly 100 FRBs published so far<sup>1</sup>

(Petroff et al. 2016), around ten have been localised to a host galaxy (Chatterjee et al. 2017; Bannister et al. 2019; Ravi et al. 2019; Prochaska et al. 2019; Marcote et al. 2020; Macquart et al. 2020), confirming their extragalactic origins. Some FRBs have also been observed to repeat; the first discovered, and most observed so far, is FRB 121102 (Spitler et al. 2016), and more repeating FRBs have been detected by the Canadian Hydrogen Intensity Mapping Experiment (CHIME) radio

Corresponding author: G. H. Hilmarsson  
henning@mpifr-bonn.mpg.de

<sup>1</sup> frbcat.org

telescope (CHIME/FRB Collaboration et al. 2019a,b; Fonseca et al. 2020) and the Australian Square Kilometre Array Pathfinder (ASKAP, e.g. Kumar et al. 2019).

Polarisation properties of FRBs can reveal the nature of their local environment, as well as the FRB emission process and its geometry, thus adding constraints to progenitor theories. Polarisation fractions and rotation measures (RMs) have been determined for 20 FRBs (Petroff et al. 2016). Linear polarisation fractions ranging from  $\sim 0$  to  $\sim 100\%$  have been measured, and the absolute RM values are in the range  $\sim 10$ – $500 \text{ rad m}^{-2}$ , with the exception of FRB 121102, which has an exceptionally high RM of  $\sim 10^5 \text{ rad m}^{-2}$ . FRB 121102’s RM has also proven to be highly variable, with a decrease of  $\sim 10\%$  between epochs separated by seven months (Michilli et al. 2018a). To be able to observe such a high RM, a narrow channel bandwidth or a high observing frequency are required in order to avoid intra-channel depolarisation. Typical pulsar instrumentation has channel bandwidths of  $\sim 1 \text{ MHz}$ , so high frequency observations are required to observe high RMs.

In the original discovery of FRB 121102, the dispersion measure (DM) was found to be  $557 \pm 2 \text{ pc cm}^{-3}$  (Spitler et al. 2014). In more recent observations, FRB 121102 has exhibited an increase in the measured DM,  $560.6 \pm 0.1 \text{ pc cm}^{-3}$  at 1.4 GHz in Hessels et al. (2019) and  $563.6 \pm 0.5 \text{ pc cm}^{-3}$  at 0.6 GHz in Josephy et al. (2019), revealing an average increase of roughly  $1 \text{ pc cm}^{-3}$  per year.

Bursts from FRB 121102 have been detected at frequencies spanning from  $\sim 0.3$ – $8 \text{ GHz}$  (Chawla et al. 2020; Gajjar et al. 2018). The bursting activity of FRB 121102 does not seem to follow a Poissonian process, but rather goes through phases of bursting activity and quiescence which can be better explained with a Weibull distribution (Oppermann et al. 2018). This dichotomy in activity could also be explained by the recently discovered apparent periodicity of FRB 121102 of 161 days with an active window of 54% (Rajwade et al. 2020; Cruces et al. 2020), also detected in the repeating FRB 180916.J1058+65 with a period of 16 days and a 31% activity window (Chime/Frb Collaboration et al. 2020).

FRB 121102 is the first repeating FRB to be unambiguously localised to a host galaxy (Chatterjee et al. 2017), which is a low-metallicity dwarf galaxy at a redshift of  $z = 0.193$  (Tendulkar et al. 2017) with a stellar mass of  $M_* \sim 1.3 \times 10^8 M_\odot$  and a star formation rate of  $0.23 M_\odot$  per year (Bassa et al. 2017). FRB 121102 is also coincident with a compact persistent radio source whose projected offset is  $< 40 \text{ pc}$  (Marcote et al. 2017).

The properties of FRB 121102 and its persistent radio source have motivated a number of FRB models.

Among the leading scenarios, FRBs are generated by flaring magnetars within supernova remnants (SNRs). Here, the magnetar flares collide with the surrounding medium, producing shocks creating synchrotron maser emission, resulting in FRB generation. The main difference between these models lies in the nature of the shocked material, being dominated by either the magnetar wind nebula (e.g. Lyubarsky 2014), or by previous magnetar flares (e.g. Beloborodov 2017, 2019; Margalit & Metzger 2018).

In this work we have observed FRB 121102 with the 305-m William E. Gordon Telescope at the Arecibo Observatory (AO) in Puerto Rico, USA, the Effelsberg 100-m Radio Telescope in Effelsberg, Germany, and the Karl G. Jansky Very Large Array (VLA) in New Mexico, USA, to obtain RMs from its bursts in order to investigate its long-term RM evolution. In §2 we describe our observations, data acquisition and search analysis. In §3 we report sixteen new RM measurements of FRB 121102, a long-term average FRB 121102 burst rate from our Effelsberg observations, and discuss the properties of the detected bursts. §4 is dedicated to comparing our results to the theoretical prediction of the RM evolution of an SNR from the works of Piro & Gaensler (2018) and Margalit & Metzger (2018), as well as the Galactic center (GC) magnetar, PSR J1745–2900 (Desvignes et al. 2018), and in §5 we interpret those results. Finally, in §6 we summarise our findings.

## 2. OBSERVATIONS

The observational setup and the data processing of each telescope used in this work is detailed in their respective subsections below.

We anticipated extremely high RM values from FRB 121102 bursts, and have thus observed at frequencies higher than the 1.4-GHz band in order to avoid intra-channel depolarisation.

### 2.1. Arecibo

Data from the 305-m William E. Gordon Telescope at the Arecibo Observatory were acquired by using the C-band receiver at an observing frequency between 4.1 and 4.9 GHz, composed of two orthogonal linear-polarization feeds. The Puerto Rican Ultimate Pulsar Processing Instrument (PUPPI) backend recorded dual-polarisation data every  $10.24 \mu\text{s}$  in 512 frequency channels, each coherently dedispersed to  $\text{DM} = 557 \text{ pc cm}^{-3}$  to reduce intra-channel dispersive smearing to  $< 2 \mu\text{s}$ . The time and frequency resolution were reduced to  $81.92 \mu\text{s}$  and  $12.5 \text{ MHz}$ , respectively, before searching for bursts. We

used PRESTO<sup>2</sup> (Ransom 2011) to create 200 dedispersed time-series between 461 and 661 pc cm<sup>-3</sup>, which were searched by `single_pulse_search.py` with box-car filters ranging from 81.92  $\mu$ s to 24.576 ms. A large fraction of detections due to noise and radio frequency interference (RFI) were excluded by using dedicated software<sup>3</sup> (Michilli et al. 2018b). A ‘waterfall’ plot of signal intensity as a function of time and frequency was produced and visually inspected for the rest of the detections. The DSPSR package<sup>4</sup> (van Straten & Bailes 2011) was used to create PSRCHIVE<sup>5</sup> (Hotan et al. 2004) files containing the full resolution data recorded by PUPPI.

For each observation, the differential gain of the two receiver feeds was corrected for by analyzing with PSRCHIVE utilities a one-minute noise injection performed with a diode. Additional calibrations, such as observations of a calibration source, were not performed and residual artifacts in the measured polarization fraction may be present. RM values were calculated by using a technique called RM synthesis (Burn 1966; Brentjens & de Bruyn 2005), which reconstructs the Faraday dispersion function (FDF) of a source through a Fourier transform, in the implementation included in the `RM-tools` package.<sup>6</sup> We cleaned the resulting FDF by using a deconvolution algorithm (Heald 2009). RM uncertainties are estimated from the width of the peak in the FDF, rescaled by the maximum S/N. The FDF of bursts detected on MJDs 58222 and 58712 (bursts 8, 19 and 20) shows signs of a poor polarisation calibration, namely symmetric RM peaks around the origin. This is likely caused by a delay calibration issue and, while the RM measurements are still valid, the resulting linear polarisation fractions should be considered lower limits. Conversely, the lack of an RM=0 rad m<sup>-2</sup> peak for the bursts with  $\sim 100\%$  linear polarisation fractions indicates that cross-coupling between the X and Y polarisations does not have a significant effect on our results. For these bursts, we also find no evidence for significant circular polarisation varying with radio frequency, which can occur if there is cross-coupling and poor calibration. PA curves were calculated by de-rotating the data with PSRCHIVE at the RM value obtained for each burst.

## 2.2. Effelsberg

We have used the Effelsberg 100-m radio telescope to observe FRB 121102 at 4–8 GHz using the S45mm re-

ceiver with a roughly two-week cadence for 2–3 hours each session from late 2017 to early 2020, totaling 115 hours. The S45mm receiver has dual linear polarisation feeds.

The data were recorded with full Stokes information using two ROACH2 backends with each one capturing 2 GHz of the band. The channel bandwidth is 0.976562 MHz across 4096 channels, with a 131  $\mu$ s sampling rate. The recorded data were in a Distributed Acquisition and Data Analysis (DADA) format<sup>7</sup>. Before processing, Stokes *I* was extracted from the data into a SIGPROC filterbank<sup>8</sup> format in order to perform the initial burst searching.

Observations on 22nd October 2018 encountered a receiver issue, forcing us to use the S60 mm receiver instead. The S60 mm receiver has an SEFD of 18 Jy, 500 MHz of bandwidth from 4.6 to 5.1 GHz, 0.976562 MHz channel bandwidth across 512 channels, and an 82  $\mu$ s sampling rate. The data were recorded as SIGPROC filterbanks.

The data were searched for single pulses using the PRESTO software package. We used `rfifind` to identify RFI in the data over two-second intervals and to make an RFI mask which was applied to the data during searching. We used PRESTO to create dedispersed time-series of the data from 0–1000 pc cm<sup>-3</sup> in steps of 2 pc cm<sup>-3</sup>, which were searched for single pulses using `single_pulse_search.py` to convolve the time-series with boxcar filters of varying widths to optimise the signal-to-noise of a burst. A pre-determined list of boxcar widths from PRESTO was used, where the widths are multiples of the data sampling time. We searched for burst widths up to 19.6 ms and applied a signal-to-noise threshold of 7. DM-time and frequency-time plots of candidates were visually inspected to search for bursts.

For further RFI mitigation we calculated the modulation index of candidates. The modulation index assesses a candidate’s fractional variations across the frequency channels in order to discriminate between narrowband RFI and an actual broadband signal (Spitler et al. 2012). We applied this thresholding following Hilmarsson et al. (2020).

If a burst was detected, we performed polarisation calibration in order to obtain the RM, polarisation angle (PA), and degree of polarisation of the burst. We used the `psrfits_utils` package<sup>9</sup> to create a `psrfits`<sup>10</sup> file

<sup>2</sup> [github.com/scottransom/presto](https://github.com/scottransom/presto)

<sup>3</sup> <http://ascl.net/1806.013> (Michilli & Hessels 2018)

<sup>4</sup> <http://dspsr.sourceforge.net/>

<sup>5</sup> <http://psrchive.sourceforge.net/>

<sup>6</sup> <https://github.com/CIRADA-Tools/RM-Tools>

<sup>7</sup> <http://psrdada.sourceforge.net>

<sup>8</sup> <http://sigproc.sourceforge.net>

<sup>9</sup> [github.com/demorest/psrfits\\_utils](https://github.com/demorest/psrfits_utils)

<sup>10</sup> [atnf.csiro.au/research/pulsar/psrfits.definition/Prsfits.html](http://atnf.csiro.au/research/pulsar/psrfits.definition/Prsfits.html)

containing the burst and used `PSRCHIVE` to calibrate the data by first dedispersing the burst data using `pam`, then `pac` to polarisation calibrate those data with noise diode observations. RM was obtained using RM synthesis, described in §2.1.

### 2.3. VLA

FRB 121102 was observed with the VLA as part of a monitoring project (VLA/17B-283) from 2017 November to 2018 January. Ten 1-hr observations were conducted at 2–4 GHz using the phased-array pulsar mode. The VLA has dual circular polarisation feeds. Data were recorded with full Stokes information with  $8096 \times 0.25$  MHz channels and 1024  $\mu$ s time samples. Each observation had  $\approx 30$  min on-source. Data were dedispersed at 150 trial DMs from  $400 - 700$  pc cm $^{-3}$  and the resulting time-series were searched for pulses using the `PRESTO single_pulse_search.py`.

Polarisation calibration was done using the 10-Hz injected noise calibrator signal. After polarisation calibration, the RMs were obtained using RM synthesis, as described in §2.1.

## 3. OBSERVATIONAL RESULTS

From our observations we have sixteen new RM measurements from FRB 121102 bursts: 1 from Effelsberg, 2 from the VLA, and 13 from Arecibo. The details of our detections, along with previously reported RM values, are listed in Table 1. The previously reported RM values from Arecibo (Michilli et al. 2018a) and the GBT (Gajjar et al. 2018) listed in Table 1 are a global fit to multiple bursts from the same epoch. Each burst is also assigned a numerical value for clarity. The burst DMs in Table 1 are obtained from L-band bursts detected at Arecibo by linearly interpolating their four-week averaged DM values, producing a mode error value of  $0.14$  pc cm $^{-3}$  for the interpolated values (Seymour et al., in prep.). The L-band burst DMs were determined by maximising the structure of the bursts and their sub-component alignment<sup>11</sup>.

### 3.1. Long-term Burst Rate at C-band at Effelsberg

Previous surveys of FRB 121102 at frequencies between 4–8 GHz reported rates based on fewer observed hours (Spitler et al. 2018) and anomalously high burst rates (Gajjar et al. 2018). Spitler et al. (2018) detected three bursts from observing at 4.6–5.1 GHz for 22 hours consisting of 10 observing epochs spanning five months using the Effelsberg telescope. Gajjar et al. (2018) de-

tected 21 bursts in a single six-hour observation, observing at 4–8 GHz at the Green Bank Telescope. Furthermore, Zhang et al. (2018) re-searched the data from Gajjar et al. (2018) using a convolutional neural network and detected an additional 72 bursts within the data.

Our Effelsberg survey spans over two years of observing FRB 121102 for 2–6 hrs at a time at 4–8 GHz with a two-week cadence, amounting to 115 hours of observations. Included here are 10 hours of observations presented in Caleb et al. (2020). We can therefore report a robust, long-term average burst rate of FRB 121102 in this frequency range of  $0.21^{+0.49}_{-0.18}$  bursts/day (1-sigma error) above a fluence of  $0.04$  ( $w/ms$ ) $^{1/2}$  Jy ms for a burst width of  $w$  ms. We list the details of the surveys discussed here in Table 2.

A caveat to our observed burst rate is the suspected periodic activity of FRB 121102 (Rajwade et al. 2020). Roughly 40% of our Effelsberg observations were performed during suspected inactivity of FRB 121102, which if true would affect the observed burst rate. No bursts were detected during this state of inactivity. Including only observations while FRB 121102 is active, the average burst rate becomes  $0.35^{+0.80}_{-0.29}$  bursts/day above a fluence of  $0.04$  ( $w/ms$ ) $^{1/2}$  Jy ms.

The observed burst rates of FRB 121102 also seem to be frequency dependent, with the rate being lower at higher frequencies. At 1.4 GHz the FRB 121102 burst rate has been observed to be  $8 \pm 3$  bursts/day above a fluence of  $0.08$  Jy ms for 1 ms burst widths (Cruces et al. 2020).

### 3.2. Burst Properties

We plot the dynamic spectra, polarisation profile, and polarisation angles (PAs) of our detected bursts in Fig. 1. The PA is equal to  $RM\lambda^2 + PA_{\text{ref}}$ , where  $\lambda$  is the observing wavelength, and  $PA_{\text{ref}}$  is a reference angle at a specific frequency (central observing frequency in our case). The PAs are flat across each burst, as has been seen previously from FRB 121102 (Michilli et al. 2018a; Gajjar et al. 2018). We do not discuss PA changes over time, as we did not observe an absolute calibrator for polarisation. In the absence of an absolute calibrator we cannot compare PAs across multiple telescopes, and a more detailed discussion is outside the scope of this work.

The bursts are mostly  $\sim 100\%$  linearly polarised. Bursts from FRB 121102 have been consistently  $\sim 100\%$  linearly polarised since its first polarisation measurement in late 2016 (Michilli et al. 2018a), which suggests a stability in its emission process. The Arecibo bursts at MJD 58222, 58247, and 58712 (bursts 8, 15, 19, and 20) are not fully linearly polarised, which is uncharacteristic

<sup>11</sup> <http://ascl.net/1910.004> (Seymour et al. 2019)

**Table 1.** Burst detections of FRB 121102 with measured RMs in chronological order. *From left to right:* Burst number, barycentric burst arrival time in MJD (referenced to infinite frequency), width ( $w$ , full-width at half-maximum), flux density ( $S$ ), fluence ( $F$ ), observed RM, DM, observing frequency, and telescope used. The burst DMs are approximated by linearly interpolating the four-week averaged DM values of the L-band bursts detected at Arecibo. This produces a mode error value of  $0.14 \text{ pc cm}^{-3}$  for the interpolated values. The initial L-band DM values are determined by maximising their burst and sub-component alignment. Sub-bursts of multi-component bursts are further labeled chronologically with lower-case letters. Previously reported bursts and bursts introduced in this work are separated by a horizontal line. Abbreviations are AO: Arecibo Observatory, Eff: Effelsberg, GBT: Green Bank Telescope, VLA: Very Large Array.

Burst	MJD	$w$ (ms)	$S$ (Jy)	$F$ (Jy ms)	RM <sub>obs</sub> (rad m <sup>-2</sup> )	DM (pc cm <sup>-3</sup> )	Freq. (GHz)	Telescope
1	57747.12956–57747.17597				102708(4)		4.1–4.9	AO <sup>a,c</sup>
2	57748.12564–57748.17570				102521(4)		4.1–4.9	AO <sup>a,c</sup>
3	57772.12903030				103039(4)		4.1–4.9	AO <sup>a</sup>
4	57991.58013–57991.58330				93573(24)		4–8	GBT <sup>a,b,c</sup>
5	58069.31853200	$4.49 \pm 0.09$	$0.38 \pm 0.06$	1.69	86678(3)	560.5	2–4	VLA
6a		$1.65 \pm 0.07$	$0.16 \pm 0.02$	0.26				
6b	58075.20058018	$1.95 \pm 0.08$	$0.32 \pm 0.05$	0.63	86518(3)	560.6	2–4	VLA
6c		$3.62 \pm 0.08$	$0.56 \pm 0.08$	2.03				
7	58215.86332798	$0.34 \pm 0.01$	$0.19 \pm 0.03$	0.06	70841(38)	561.5	4.1–4.9	AO
8a	58222.85751812	$0.59 \pm 0.01$	$0.32 \pm 0.05$	0.19	72090(22)	561.5	4.1–4.9	AO
8b		$0.34 \pm 0.04$	$0.05 \pm 0.01$	0.02				
9	58227.83201090	$0.76 \pm 0.04$	$0.08 \pm 0.01$	0.06	72062(62)	561.6	4.1–4.9	AO
10	58228.63801964	$0.69 \pm 0.08$	$0.35 \pm 0.05$	0.24	72248(21)	561.6	4–8	Eff
11	58234.81180934	$0.39 \pm 0.03$	$0.09 \pm 0.01$	0.04	73514(75)	561.6	4.1–4.9	AO
12	58234.81642918	$0.35 \pm 0.01$	$0.20 \pm 0.03$	0.07	73358(38)	561.6	4.1–4.9	AO
13	58243.77965432	$0.52 \pm 0.01$	$1.8 \pm 0.3$	0.96	71525(3)	561.7	4.1–4.9	AO
14a	58244.77641721	$0.92 \pm 0.03$	$0.13 \pm 0.02$	0.12	71158(33)	561.7	4.1–4.9	AO
14b		$0.69 \pm 0.03$	$0.12 \pm 0.02$	0.08				
15	58247.81273381	$0.54 \pm 0.02$	$0.13 \pm 0.02$	0.07	68937(72)	561.7	4.1–4.9	AO
16	58677.60475978	$0.30 \pm 0.02$	$0.13 \pm 0.02$	0.04	69375(43)	563.3	4.1–4.9	AO
17	58684.58367814	$0.47 \pm 0.03$	$0.09 \pm 0.01$	0.04	69524(58)	563.2	4.1–4.9	AO
18	58684.58990897	$0.25 \pm 0.02$	$0.09 \pm 0.01$	0.02	69408(92)	563.2	4.1–4.9	AO
19a	58712.47972031	$0.90 \pm 0.03$	$0.27 \pm 0.04$	0.24	66949(11)	563.1	4.1–4.9	AO
19b		$0.207 \pm 0.001$	$1.9 \pm 0.3$	0.40				
20	58712.48531398	$1.89 \pm 0.09$	$0.06 \pm 0.01$	0.11	67033(87)	563.1	4.1–4.9	AO

<sup>a</sup>Results presented in Michilli et al. (2018a).

<sup>b</sup>Results presented in Gajjar et al. (2018).

<sup>c</sup>Global fit to multiple bursts.

**Table 2.** FRB 121102 surveys at frequencies between 4–8 GHz. *From left to right:* Survey, number of bursts, number of hours observed, number of observing epochs, frequency range, and telescope used. All surveys except Spitler et al. (2018) recorded full Stokes data. Abbreviations are AO: Arecibo Observatory, Eff: Effelsberg, GBT: Green Bank Telescope.

Survey	No. bursts	No. hours	No. epochs	Freq. (GHz)	Telescope
Spitler et al. (2018)	3	22	10	4.6–5.1	Eff
Michilli et al. (2018a)	16	13	12	4.1–4.9	AO
Gajjar et al. (2018)	21	6	1	4–8	GBT
Zhang et al. (2018) <sup>a</sup>	93	6	1	4–8	GBT
This work	1	115	35	4–8	Eff

<sup>a</sup>Re-searching of data from Gajjar et al. (2018)

for FRB 121102, and can be attributed to polarisation calibration issues (see §2.1).

The circular polarisation fraction is on average 4% for all the bursts and 17% by summing the absolute Stokes  $V$  values. The Stokes  $V$  on-pulse and off-pulse standard deviation is the same for the majority of the bursts, indicating that the circular polarisation is consistent with noise, therefore the circular polarisation fractions quoted above are upper limits. For the VLA and Effelsberg bursts (number 5, 6, and 10) the on and off-pulse statistics differ, where the on-pulse standard deviation is larger by a factor of two, and we obtain circular polarisation fractions for Stokes  $V$  and absolute Stokes  $V$  of 5%/5%, 2%/4%, and 3%/11% for bursts 5, 6, and 10, respectively. The 100% linear polarisation and the lack of circular polarisation for the majority of bursts indicates that little to no Faraday rotation conversion, where linear polarisation is converted to circular in a magneto-ionic environment (Vedantham & Ravi 2019; Gruzinov & Levin 2019), occurs at our observing frequencies.

The VLA burst on MJD 58075 (burst 6) exhibits a triple component profile. The second and third components exhibit a downward drift in frequency, a feature predominantly observed from repeating FRBs (e.g. Hessels et al. 2019; The CHIME/FRB Collaboration et al. 2020). An apparent upward drift in frequency between the first two components can be seen, and the first component has a different PA than the other two. While the temporal spacing between the components is not large, the difference in PAs between the first component and the other two might suggest that these are in fact two separate bursts.

The Effelsberg burst at MJD 58228 (burst 10) was only detected between 4–5.2 GHz of the 4–8 GHz bandwidth. We were affected by strong edge effects in the bandpass, resulting in an uneven frequency response across the bandwidth. Thus we are uncertain of whether the burst frequency envelope is inherent to the burst or due to the bandpass.

### 3.3. Dispersion and Rotation Measures of FRB 121102

The RMs we obtained from our bursts are listed in Table 1. We plot the RMs over time in Fig. 2. The observed RM of FRB 121102 has dropped by 34% over 2.6 years from  $\sim 10^5$  rad m $^{-2}$  to  $\sim 6.7 \times 10^4$  rad m $^{-2}$ . As Fig. 2 shows, the drop in RM has not been steady over time. From MJD 57757 to MJD 58215 (bursts 1–7), the RM decreased rapidly to  $\sim 7 \times 10^4$  rad m $^{-2}$  and has declined only slightly ( $\sim 5000$  rad m $^{-2}$ ) since then. An FDF plot of the bursts reported here can be seen in Fig. 3.

Within a 32-day timespan the observed RM of FRB 121102 exhibited significant short-timescale variations (bursts 7–15). At epochs separated by a week, the RM increased by  $\sim 1000$  rad m $^{-2}$  (bursts 7–8). For three epochs during the following week, the RM remained stable between bursts 8–10, before increasing again by  $\sim 1000$  rad m $^{-2}$  a week later (bursts 11–12). During three epochs in the following two weeks, the RM was observed to drop rapidly by a total of  $\sim 4500$  rad m $^{-2}$  (bursts 12–15). This short-timescale behaviour can be seen in the inset of Fig 2. No RM measurement is available between MJDs 58247 and 58677 (430 days), but the RMs are consistent with each other at these dates (bursts 15–16). Another drop in RM of  $\sim 2000$  rad m $^{-2}$  can be seen between bursts 18 and 19, separated by 28 days.

Only minor changes in DM have been observed during the observed RM evolution of FRB 121102. While the RM decreased significantly, the DM has increased by  $\sim 4$  pc cm $^{-3}$ , from  $559.7 \pm 0.1$  pc cm $^{-3}$  (Michilli et al. 2018a) up to 563.3 pc cm $^{-3}$  from the aforementioned linear interpolation of L-band burst DMs used in this work.

Michilli et al. (2018a) constrained the average magnetic field along the LoS in the region which Faraday rotation occurs,  $\langle B_{\parallel} \rangle$ , between 0.6 mG and 2.4 mG using their measured FRB 121102 RM in the source frame of  $\text{RM}_{\text{src}} \sim 1.4 \times 10^5$  rad m $^{-2}$  and the estimated host DM contribution of  $\text{DM}_{\text{host}} 70\text{--}270$  pc cm $^{-3}$  (Tendulkar et al. 2017). From a measured DM and RM,  $\langle B_{\parallel} \rangle$  can be calculated, ignoring sign reversals, as

$$\langle B_{\parallel} \rangle = 1.23 \text{ RM}_{\text{src}} / \text{DM}_{\text{host}} \mu\text{G}. \quad (1)$$

The most recent DM and RM values in our sample yield  $\langle B_{\parallel} \rangle = 0.4\text{--}1.6$  mG. This is a lower limit as the DM in the Faraday rotating region could be much lower.

## 4. IMPLICATIONS FOR SOURCE SCENARIOS

We explore two models which estimate the RM evolution over time within an SNR. First is a model from Piro & Gaensler (2018) which estimates both the RM and DM evolution for three different scenarios: a supernova expanding into a constant density ISM, a progenitor wind affecting the circumstellar medium, solely contributing to the RM, and a supernova expanding into wind affected ISM. The second model is a one-zone magnetar nebula expanding spherically at a constant radial velocity (Margalit & Metzger 2018). Each model is described in more detail in Appendix A.

Additionally, we consider an environment near a massive black hole by comparing to the GC magnetar, PSR J1745–2900. The RM magnitude and trend of

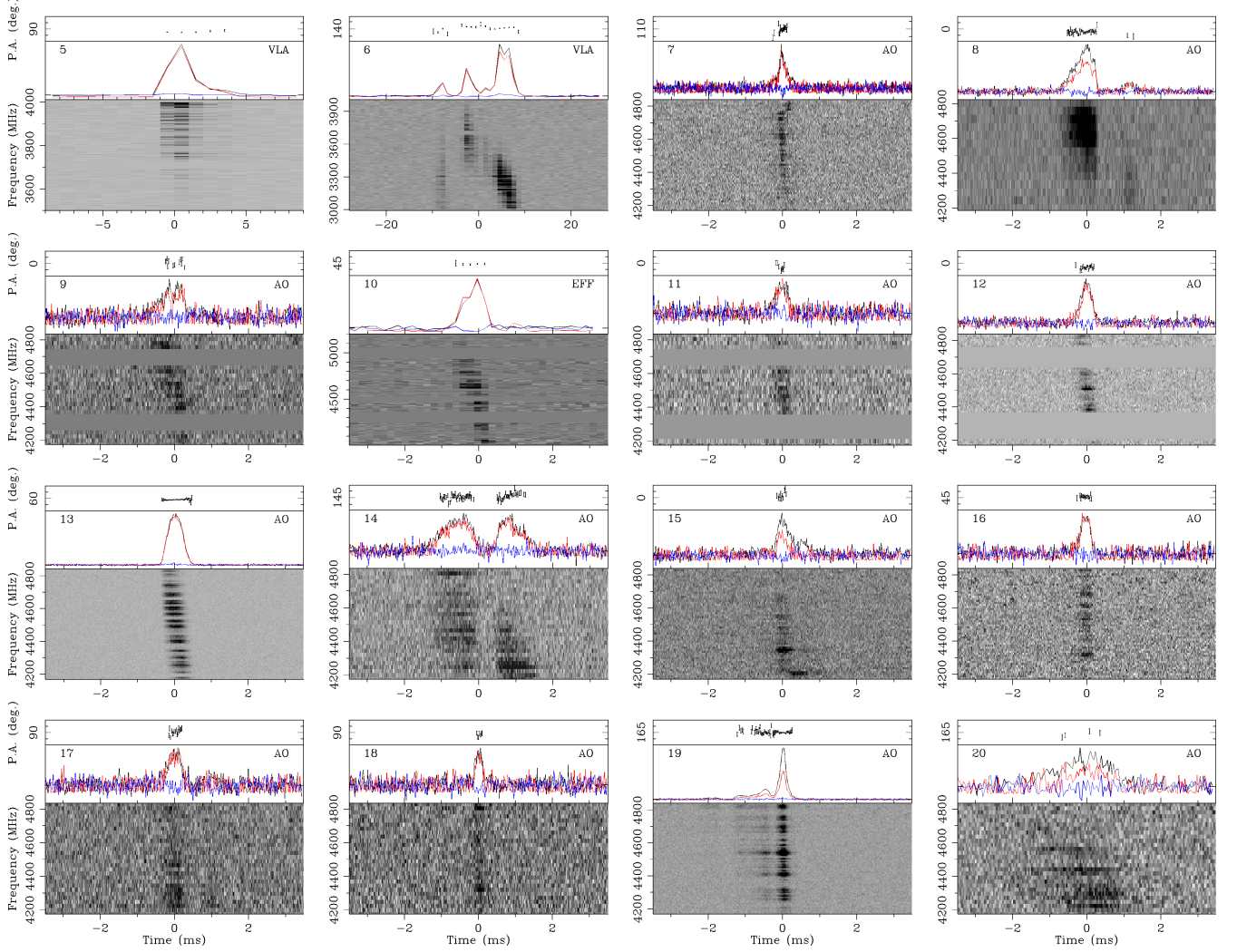


**Figure 1.** Dynamic spectra of the bursts detected with Arecibo, VLA, and Effelsberg in a chronological order, dedispersed to their respective DMs listed in Table 1. On top of each spectrum is plotted the profile of the burst (in black), linear polarisation (red), and circular polarisation (blue), as well as the polarisation angle (PA). The PA range in each panel is 60 degrees. Each panel is labeled with the corresponding burst number from Table 1 and the telescope at which the burst was detected. Bursts 8, 15, 19, and 20 suffer from delay calibration issues, resulting in unreliable polarisation fractions (see §2.1).

FRB 121102 seems to be analogous to PSR J1745–2900, which has undergone rapid changes in RM in recent times (Desvignes et al. 2018).

Using Bayesian inference, we fit the RM evolution prediction from the aforementioned SNR models to the observed RM of FRB 121102. A Markov-chain Monte Carlo (MCMC) method is used to estimate the posterior of the model parameters and the age of the FRB 121102 bursting source,  $t_{\text{age}}$ , at the time of its first RM measurement. The models considered here predict that DM decreases over time, while the observed DM is increasing. We therefore do not perform a similar analysis on the DM evolution. The models do not take into account the short-term stochasticity in RM that we observe and our RM uncertainties are also relatively small. We therefore

introduce an error added in quadrature in our fitting,  $\Sigma$ , to allow for a broader exploration of the free parameter space in our MCMC and to obtain more conservative uncertainties on the model parameters. Further details on the fitting can be found in Appendix B.

Henceforth, all values mentioned will be in the reference frame of the source, unless otherwise stated. This requires a conversion of the observed values to the source frame. The conversions are  $\text{DM}_{\text{source}} = \text{DM}_{\text{obs}}(1+z)$ ,  $\text{RM}_{\text{source}} = \text{RM}_{\text{obs}}(1+z)^2$ , and  $t_{\text{source}} = t_{\text{obs}}(1+z)^{-1}$ , where  $z \sim 0.2$  is the redshift of FRB 121102. This means that the minimum  $t_{\text{age}}$  possible in the source frame at the time of the first RM measurement is just over 3 years due to the time elapsed from the first detection of FRB 121102 (Spitler et al. 2014) and its first RM mea-

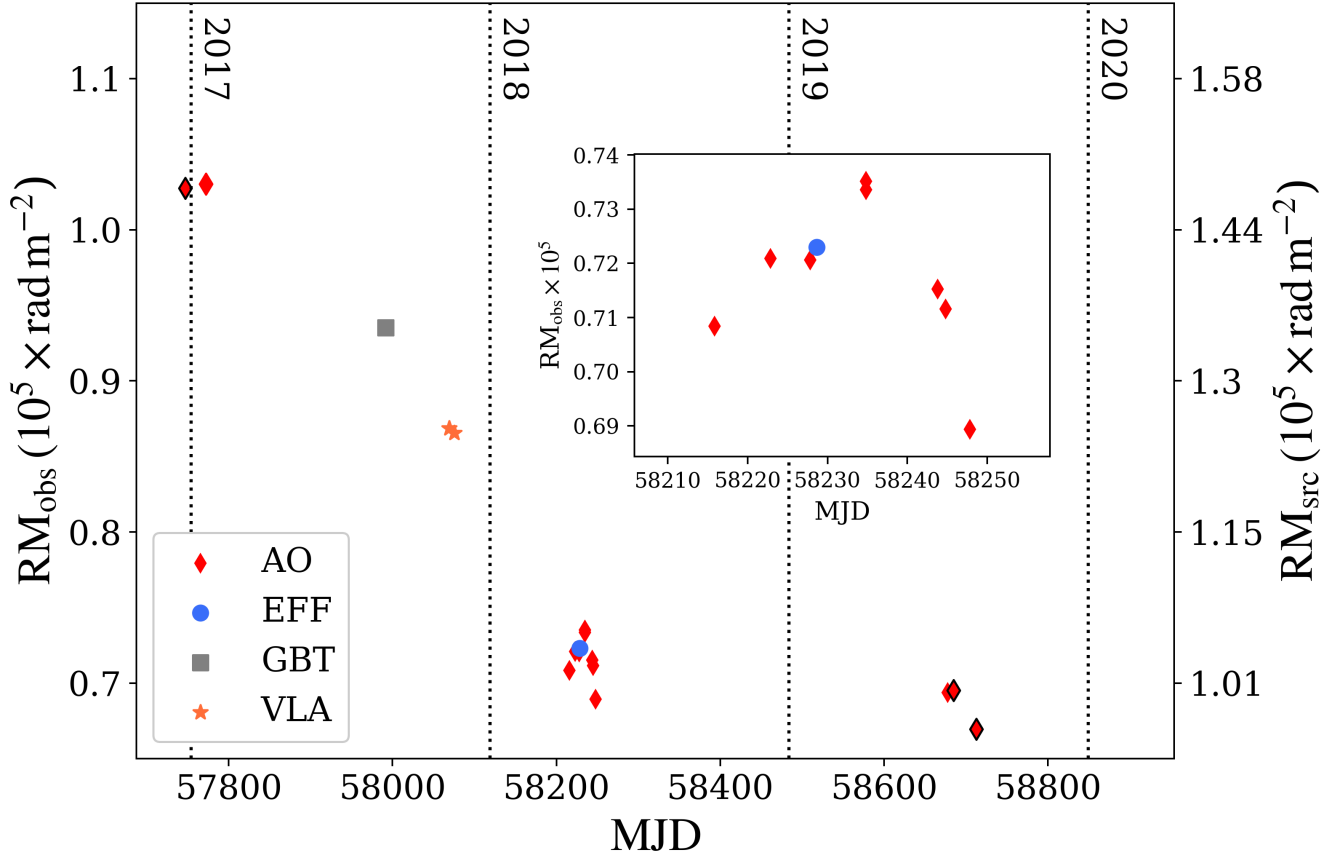


**Figure 2.** The 20 RMs of FRB 121102 as a function of time in MJD. The left y-axis shows the observed RM and the right y-axis shows the RM in the source frame of FRB 121102. Different markers indicate at which telescope the burst was detected. Markers with a black edge indicate two bursts whose markers would otherwise overlap due to being too close in time and RM. The horizontal dotted lines show the start of each calendar year. The inset gives a closer look at the cluster of bursts around MJD  $\sim 58230$  (when a high-cadence observing campaign was performed). The observed rotation measure uncertainties are not large enough to exceed the boundaries of the markers. Abbreviations are AO: Arecibo Observatory, Eff: Effelsberg, GBT: Green Bank Telescope, VLA: Very Large Array. The points near MJD 57800 and 58000 are data from [Michilli et al. \(2018a\)](#) and [Gajjar et al. \(2018\)](#) respectively.

surement ([Michilli et al. 2018a](#)). In the case of DM, we will only consider the contribution local to the source, i. e. local to the bursting source and the host galaxy.

#### 4.1. [Piro & Gaensler \(2018\)](#)

For the constant density ISM model variety the number density of the ISM,  $n$ , is a free parameter, and for the progenitor wind model varieties the wind mass loading parameter,  $K$ , is a free parameter. For all model varieties we also set  $t_{\text{age}}$  and  $\Sigma$  as free parameters for SN ejecta masses of 10 and 2  $M_{\odot}$ . In all cases the SN explosion energy is  $10^{51}$  erg.

We estimate the posterior of  $n$ ,  $K$ ,  $t_{\text{age}}$ , and  $\Sigma$  for each model variety ([Piro & Gaensler 2018](#), Eqs. 26, 57, and Appendix) using the measured RM values of FRB 121102 (Table 1). Our initial guesses are the median values of  $n$  ( $1 \text{ cm}^{-3}$ ) and  $K$  ( $10^{13} \text{ g cm}^{-1}$ ) from [Piro](#)

& [Gaensler \(2018\)](#),  $t_{\text{age}} = 5$  years, and  $\Sigma = 10^3 \text{ rad m}^{-2}$  (roughly 1% of the observed RM magnitude). Our results are listed in Table 3.

For the constant ISM model we obtain a  $t_{\text{age}}$  of 1.4 years at the time of the first RM detection. For the wind and wind plus SNR evolution models we obtain  $t_{\text{age}}$  between  $\sim 6$ –8 years. The range of RM from our results (1-sigma error) for each model and mass is plotted as a function of time in Fig. 4, and overplotted with the observed RM values of FRB 121102.

We also plot the local DM versus RM for the models in [Piro & Gaensler \(2018\)](#) in Fig. 5, showing how the DM changes as RM decreases over time. The estimated source frame local DM (up to  $270 \text{ pc cm}^{-3}$ , [Tendulkar et al. 2017](#)) and the source frame RM values of FRB 121102 are overplotted on the figure.



**Table 3.** Model parameters of Piro & Gaensler (2018) for each scenario. *From left to right:* Model scenario, supernova explosion energy ( $E$ ), supernova ejecta mass ( $M$ ), number density of surrounding uniform ISM ( $n$ ), wind mass loading parameter ( $K$ ), age of bursting source ( $t_{\text{age}}$ ), and the factor that takes into account additional errors and astrophysical variance in RM,  $\Sigma$ . The parameters  $n$ ,  $K$ ,  $t_{\text{age}}$ , and  $\Sigma$  were obtained in this work (§4.1). Uncertainties are 1-sigma.

Model	$E$ (erg)	$M$ ( $M_{\odot}$ )	$n$ ( $\text{cm}^{-3}$ )	$\log_{10}(K)$ ( $\text{g cm}^{-2}$ )	$t_{\text{age}}$ (years)	$\log_{10}(\Sigma)$ ( $\text{rad m}^{-2}$ )
Const. ISM	$10^{51}$	10	$1.7^{+0.1}_{-0.1}$	-	$1.4^{+0.2}_{-0.2}$	$3.9^{+0.1}_{-0.1}$
	$10^{51}$	2	$2.5^{+0.1}_{-0.1}$	-	$1.4^{+0.2}_{-0.2}$	$3.8^{+0.1}_{-0.1}$
Wind	$10^{51}$	10	-	$15.3^{+0.1}_{-0.1}$	$7.8^{+0.9}_{-1.1}$	$3.9^{+0.1}_{-0.1}$
	$10^{51}$	2	-	$15.6^{+0.1}_{-0.1}$	$6.4^{+0.6}_{-0.7}$	$3.9^{+0.1}_{-0.1}$
Wind + SNR	$10^{51}$	10	-	$11.7^{+0.1}_{-0.1}$	$8.3^{+1.0}_{-1.2}$	$3.9^{+0.1}_{-0.1}$
	$10^{51}$	2	-	$11.9^{+0.1}_{-0.1}$	$8.3^{+1.0}_{-1.1}$	$3.9^{+0.1}_{-0.1}$

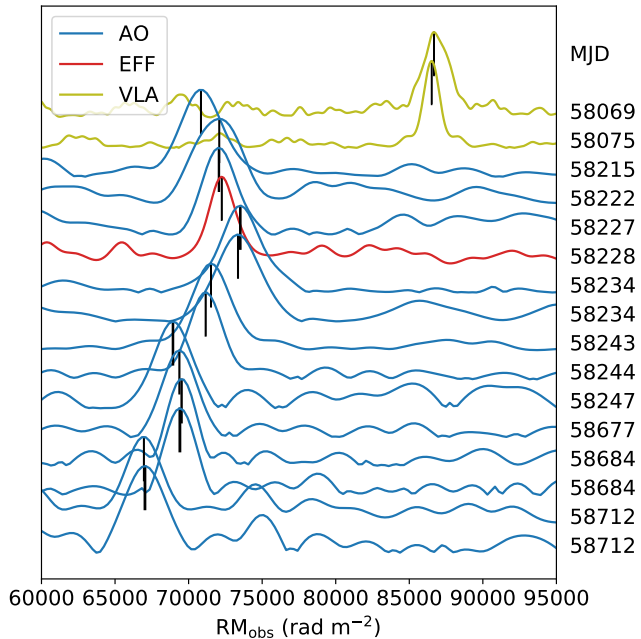


**Figure 3.** Faraday dispersion function of the bursts presented in this work, with different colors for different telescopes. Each curve is normalised to a unitary peak for clarity and the resulting RM value is indicated with a vertical black line whose thickness is the  $1-\sigma$  uncertainty. The burst MJDs are reported on the right.

#### 4.2. Margalit & Metzger (2018)

In this model we set  $t_{\text{age}}$ ,  $\Sigma$ , and the power-law parameter,  $\alpha$ , as free parameters. The free magnetic energy of the magnetar,  $E_{B_*}$ , the time since the onset of the magnetar’s activity,  $t_0$ , and the expansion velocity of the nebula,  $v_n$ , differ between model varieties ‘A, B, and C’. We estimate the posterior of  $\alpha$ ,  $t_{\text{age}}$ , and  $\Sigma$ . The initial guesses are the parameters of models A, B, and C and  $t_{\text{age}}$  in Margalit & Metzger (2018), and like before  $\Sigma = 10^3 \text{ rad m}^{-2}$ . Our results are listed in Table 4.

A similar  $t_{\text{age}}$  of  $\sim 15\text{--}17$  years was obtained for all the models. Our obtained  $\alpha$  values lie in the range of 1.1–1.6 and are consistent with the values in Margalit &

Metzger (2018). The resulting RM range (1-sigma error), overplotted with observed FRB 121102 RM values is plotted in Fig. 6.

#### 4.3. Galactic Center Magnetar PSR J1745–2900

The GC magnetar PSR J1745–2900 has exhibited similar behaviour as FRB 121102 regarding changes in RM. Since its first RM measurements of  $-67000 \text{ rad m}^{-2}$  (Eatough et al. 2013), it showed some variations in RM of a few hundred  $\text{rad m}^{-2}$  per year for a few years until its RM suddenly exhibited a steep drop in absolute magnitude (Desvignes et al. 2018). This drop in RM is similar to FRB 121102, albeit not as intense, as PSR J1745–2900 had a drop of 5% in RM over the course of a year while the RM of FRB 121102 has dropped by an average of  $15\% \text{ yr}^{-1}$  over roughly two years. Both PSR J1745–2900 and FRB 121102 exhibit short-term variations in their observed RMs. Although somewhat similar, the magnitude of the FRB 121102 variations is greater. Desvignes et al. (2018) also report a constant DM and attribute the RM evolution to the changing line of sight towards the moving magnetar where either the projected magnetic field or the GC free electron content varies.

Desvignes et al. (2018) use the measured proper motion of PSR J1745–2900 to estimate the characteristic size of magneto-ionic fluctuations to be  $\sim 2$  astronomical units (AU). Assuming the bursts from FRB 121102 originate from the magnetosphere of a neutron star with a speed of  $\sim 100 \text{ km s}^{-1}$ , the source moves a distance of 20 AU per year. The observations of PSR J1745–2900 show that spatial variations on the scale of a few to 10s of AUs are possible in the vicinity of a massive black hole. If the host of FRB 121102 also harbors a massive black hole, the variations seen in the RM of FRB 121102 could be caused by the changing medium in its accretion disk. The velocity of the medium could be much higher than in the Galactic center, contributing to the observed fluctuation.

## 5. DISCUSSION

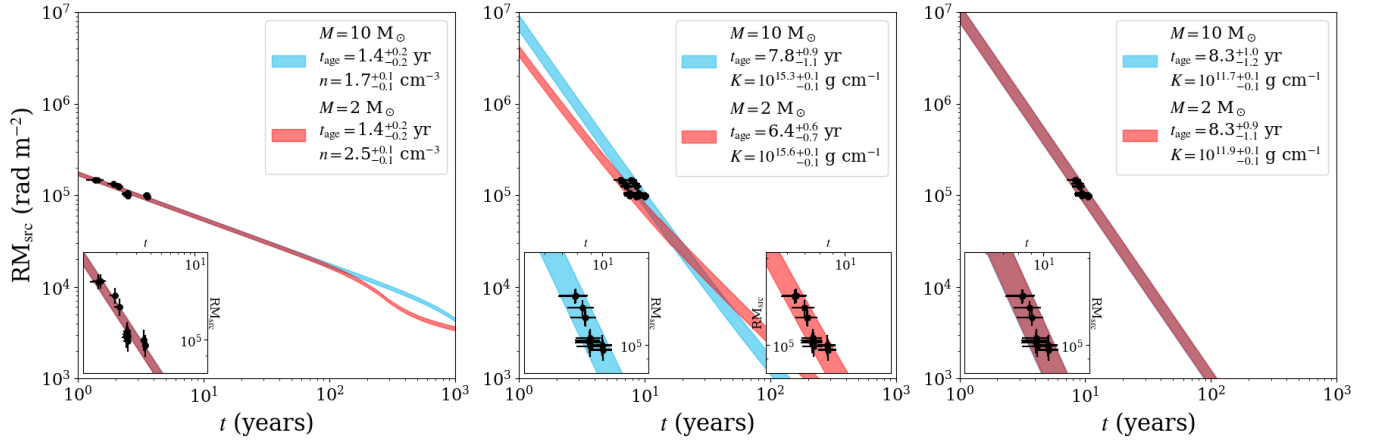


**Figure 4.** Source frame RM as a function of time for each model and ejecta mass in Piro & Gaensler (2018). The ranges show the possible RMs from the parameters obtained in this work with 1-sigma uncertainties (Table 3). The black dots are the source frame RMs of FRB 121102, starting at the obtained  $t_{\text{age}}$  for each model variation. The RM uncertainties are calculated from Eq. B3. The insets are zoomed in to the RM-time space around each  $t_{\text{age}}$ . *Left:* Uniform ISM model. *Center:* Progenitor wind model. *Right:* Progenitor wind and evolving supernova remnant model.

**Table 4.** Model parameters of Margalit & Metzger (2018). *From left to right:* Model, free magnetic energy of the magnetar ( $E_{B*}$ ), onset of magnetar’s active period ( $t_0$ ), radial velocity of expanding nebula ( $v_n$ ), power-law parameter ( $\alpha$ ) and age of bursting source ( $t_{\text{age}}$ ) used in Margalit & Metzger (2018), and  $\alpha$ ,  $t_{\text{age}}$ , and the factor that takes into account additional errors and astrophysical variance in RM,  $\Sigma$ , obtained in this work (§4.2). Uncertainties are 1-sigma.

Model	$E_{B*}$ (erg)	$t_0$ (years)	$v_n$ (cm s $^{-1}$ )	$\alpha^a$	$t_{\text{age}}$ (years) <sup>a</sup>	$\alpha^b$	$t_{\text{age}}$ (years) <sup>b</sup>	$\log_{10}(\Sigma)$ (rad m $^{-2}$ )
A	$5 \times 10^{50}$	0.2	$3 \times 10^8$	1.3	12.4	$1.6^{+0.3}_{-0.4}$	$16.8^{+2.0}_{-0.6}$	$3.9^{+0.1}_{-0.1}$
B	$5 \times 10^{50}$	0.6	$10^8$	1.3	37.8	$1.1^{+0.1}_{-0.1}$	$16.2^{+2.0}_{-2.6}$	$3.9^{+0.1}_{-0.1}$
C	$4.9 \times 10^{51}$	0.2	$9 \times 10^8$	1.83	13.1	$1.6^{+0.3}_{-0.3}$	$15.3^{+0.8}_{-0.3}$	$3.9^{+0.1}_{-0.1}$

<sup>a</sup>In Margalit & Metzger (2018)

<sup>b</sup>This work

We compared our measured RM sample to the theoretical RM predictions of Piro & Gaensler (2018) and Margalit & Metzger (2018) by obtaining MCMC posteriors of the model parameters and the age of the FRB 121102 bursting source at the time of its first RM measurement,  $t_{\text{age}}$ .

For the model variations in Piro & Gaensler (2018), we obtain a  $t_{\text{age}} \sim 1.5$  years for the uniform ISM scenario, and 6 – 9 years for the progenitor wind and progenitor wind plus SNR evolution scenarios. Based on observations, the minimum possible  $t_{\text{age}}$  is  $\gtrsim 3$  years, so we exclude the uniform ISM scenario. A drawback for the wind-only scenario is that it requires a high wind mass loading parameter ( $K > 10^{15}$  g cm $^{-1}$ ) to be consistent with the data.

We also compare our sample to the predicted DM vs RM evolution in Piro & Gaensler (2018). The excluded uniform ISM scenario predicts DM values consistent with FRB 121102, but both wind scenarios predict much higher DMs than is observed. However, all the model

variations predict a decrease rather than increase in DM at the observed source frame RMs of FRB 121102.

Our results here show that origin scenarios with standard supernovae have difficulties explaining both the RM and DM of FRB 121102. A caveat is that the models assume uniform media, while the ISM, SNR, and wind environments most likely have spatial structures such as filaments.

For the models in Margalit & Metzger (2018) we obtain a  $t_{\text{age}}$  of  $\sim 15$ – $17$  years and  $\alpha$  of 1.1–1.6. Our results show that the observed RM evolution of FRB 121102 is consistent with these models. The estimated DM contribution from the nebula in Margalit & Metzger (2018) is  $\sim 2$  –  $20$  pc cm $^{-3}$  for models A, B, and C (Eq. A2). The measured increase in DM of  $\sim 4$  pc cm $^{-3}$  is difficult to reconcile with the RM decrease if it originates from the same electrons.

An increase in DM means an increase in the LoS electron density. There are many contributing factors to the DM along the LoS, so a smaller fractional change in DM is not surprising. The Faraday rotating medium con-

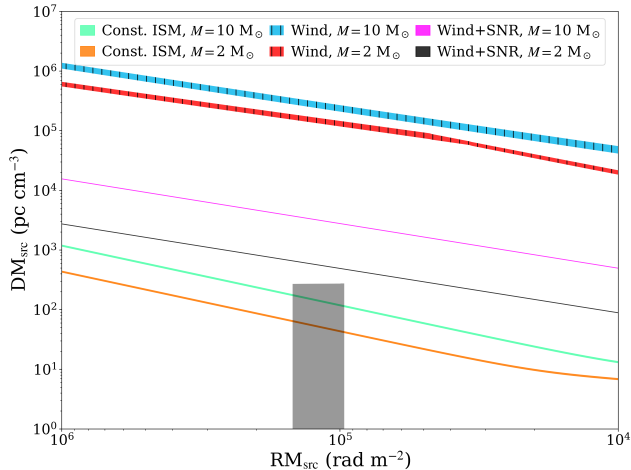


**Figure 5.** Source frame DM versus RM of each model scenario presented in Piro & Gaensler (2018). The width of each line represents the range of the predicted DMs and RMs of each scenario using the parameters obtained in this work with 1-sigma uncertainties (Table 3). The grey shaded area shows the RM and estimated local source DM contribution of FRB 121102 in the reference frame of the bursting source.

tributes only a fraction of the total DM and its amount is unknown. A decrease in RM implies a decrease in the magnetic field strength or the electron density along the LoS, or a change in the magnetic field direction. The opposing RM and DM evolution thus has two possible scenarios: the changes in RM and DM arise from different media; or the changes arise from the same medium, implying that the LoS magnetic field is decreasing in strength or changing direction.

The DM and RM might not necessarily be coupled. Metzger et al. (2019) estimate that photoionization just outside the propagating outward shock could contribute on the order of  $10 \text{ pc cm}^{-3}$  with an increase of a few  $\text{pc cm}^{-3}$  possible over several years. Therefore, the RM decrease and DM increase are likely occurring in different regions.

The SNR is initially optically thick at radio frequencies due to free-free absorption. According to Piro (2016), the SNR becomes optically thin at radio frequencies on a timescale of centuries if the SNR is solely ionised by the reverse shock. However, if the SNR is also photoionised from within by the magnetar wind nebula the SNR becomes optically thin at our observed frequencies on a timescale of  $\lesssim 10$  years (Metzger et al. 2017).

A by-product of our MCMC calculations is the error added in quadrature,  $\Sigma$ . We find  $\Sigma$  to be consistent with  $\sim 10^{3.9} \text{ rad m}^{-2}$  for all models and their variations, or roughly 10% of the observed RMs. The large value of  $\Sigma$  compared to the measured RM uncertainties could be due to deviations of the observed RMs from the RM

evolution models considered in this work, which are inherently power-laws. These deviations could be due to LoS variations across observing epochs as is seen for PSR J1745–2900 (Desvignes et al. 2018), or due to circum-source turbulence that could account for the observed stochastic and non-monotonic RM variations.

An example of RM variations from a source within an SNR is the Vela pulsar. Its RM has increased from  $34 \text{ rad m}^{-2}$  up to  $46 \text{ rad m}^{-2}$  (35% increase) and back down to  $31.4 \text{ rad m}^{-2}$  (32% decrease) between 1970 and 2004 (Hamilton et al. 1985; Johnston et al. 2005). Our estimated age of FRB 121102 is roughly three orders of magnitude less than Vela, resulting in higher turbulence and denser physical structures that could cause our observed RM variations.

PSR J1745–2900 has exhibited similarly drastic changes as FRB 121102 in RM over time (Desvignes et al. 2018). This change is attributed to variations in the projected magnetic field or the GC free electron content due to line of sight changes of the moving magnetar. FRB 121102 is located outside of its host dwarf galaxy center (Tendulkar et al. 2017), but we cannot exclude a similar scenario due to the fact that AGNs can be found offset from the optical center of dwarf galaxies (Reines et al. 2020).

A comparison can be made between FRB 121102 and another localised, repeating FRB, FRB 180916.J1058+65, which has no discernable associated persistent radio source, and its RM is three orders of magnitude less than the RM of FRB 121102. However, it can still fit within the SNR framework where the persistent radio source has faded and the RM dropped to its observed levels due to the source being a few hundred years old (Marcote et al. 2020).

The observed RMs of FRB 121102 show large-scale variations of  $\sim 10^4 \text{ rad m}^{-2}$  over year-timescales and small-scale variations of  $\sim 10^3 \text{ rad m}^{-2}$  over week-timescales. For a neutron star-black hole system, the “cosmic comb” model (Zhang 2018) predicts a periodic RM variation correlated with the orbital period of the neutron star. Such periodicities are not readily apparent in our data. There is also no obvious periodicity in the observed RM variations at the proposed FRB 121102 periodicity of 161 days (Cruces et al. 2020).

Future polarisation measurements will show whether the RM of FRB 121102 has “leveled-off” at its current magnitude or will continue to vary. If the RM continues to decrease, the parameters of the SNR models considered in this work can be constrained further. On the other hand, if the RM will stay the same, the models can be rejected or will require adjustments. If the RM

increases significantly, it would strongly challenge the SNR models.

Investigating the RM and DM evolution of repeating FRBs is certainly helpful in constraining source models. If FRBs, especially repeating ones, continue exhibiting vast differences from FRB 121102, such as host galaxy type, RM magnitude, and DM evolution, one must consider the possibility that FRB 121102 is a unique FRB source, likely residing locally to an AGN.

## 6. CONCLUSIONS

We present sixteen new RMs from bursts of FRB 121102 using observations taken with Arecibo, Effelsberg, and VLA.

Our Effelsberg survey consists of over 100 observing hours spanning over two years at 4 – 8 GHz (Table 2). An FRB 121102 survey of this magnitude in this frequency range is unprecedented, and thus enables us to present a robust, long-term average burst rate of  $0.21^{+0.49}_{-0.18}$  bursts/day above a fluence of  $0.04 (w/ms)^{1/2}$  Jy ms.

Along with previously reported RM values of FRB 121102 (Michilli et al. 2018a; Gajjar et al. 2018), we have an RM sample spanning roughly 2.5 years. During that time, the source frame RM has decreased significantly. From the first RM measurement at MJD 57747 to MJD 58215, the RM declined rapidly from  $1.4 \times 10^5$  rad m<sup>-2</sup> to  $1.0 \times 10^5$  rad m<sup>-2</sup>. From that point onward, the RM has stayed relatively constant, with only a slight decrease down to  $9.7 \times 10^4$  rad m<sup>-2</sup>. However, short-term RM variations of  $\sim 1000$  rad m<sup>-2</sup> per week have been observed during that period.

We fit the observed RM of FRB 121102 to theoretical models of RM evolution from within SNRs from Piro & Gaensler (2018) and Margalit & Metzger (2018). The results yield a source age estimate of 6–17 years for FRB 121102 at the time of its first RM measurement in late 2016. Conventional SNRs do not agree with our data, but the inclusion of a pulsar wind nebula is compatible with our data.

## ACKNOWLEDGMENTS

GHH thanks Dr. Ben Margalit for useful discussions and Dr. Nataliya K. Porayko for help with the MCMC implementation. The Arecibo Observatory is a facility of the National Science Foundation operated under cooperative agreement (#AST-1744119) by the University of Central Florida in alliance with Universidad Ana G. Méndez (UAGM) and Yang Enterprises (YEI), Inc. Based on observations with the 100-m telescope of the MPIfR (Max-Planck-Institut für Radioastronomie) at Effelsberg. The National Radio Astronomy Observatory is a facility of the National Science Foundation operated under cooperative agreement by Associated Universities, Inc. DM is a Banting Fellow. LGS is a Lise Meitner Independent Research Group leader and acknowledges support from the Max Planck Society. SH acknowledges financial support from the Deutsche Forschungsgemeinschaft (DFG) under grant BR2026/25. RSW acknowledges financial support by the European Research Council (ERC) for the ERC Synergy Grant BlackHole-Cam under contract no. 610058. R.M. recognizes support from the Queen Elizabeth II Graduate Scholarship and the Lachlan Gilchrist Fellowship. J.W.T.H. acknowledges funding from an NWO Vici grant (“AstroFlash”). This publication has received funding from the European Union’s Horizon 2020 research and innovation programme under grant agreement No 730562 [RadioNet]. We thank the anonymous referee for their insightful comments.

*Facilities:* Arecibo, Effelsberg, VLA

*Software:* Presto (Ransom 2011), psrfits\_utils, PSRchive (Hotan et al. 2004), RMsyn.py, Single-pulse searcher (Michilli et al. 2018b), DSPSR (van Straten & Bailes 2011), RM-tools, DM\_phase (Seymour et al. 2019), emcee (Foreman-Mackey et al. 2013), scipy (Virtanen et al. 2020)

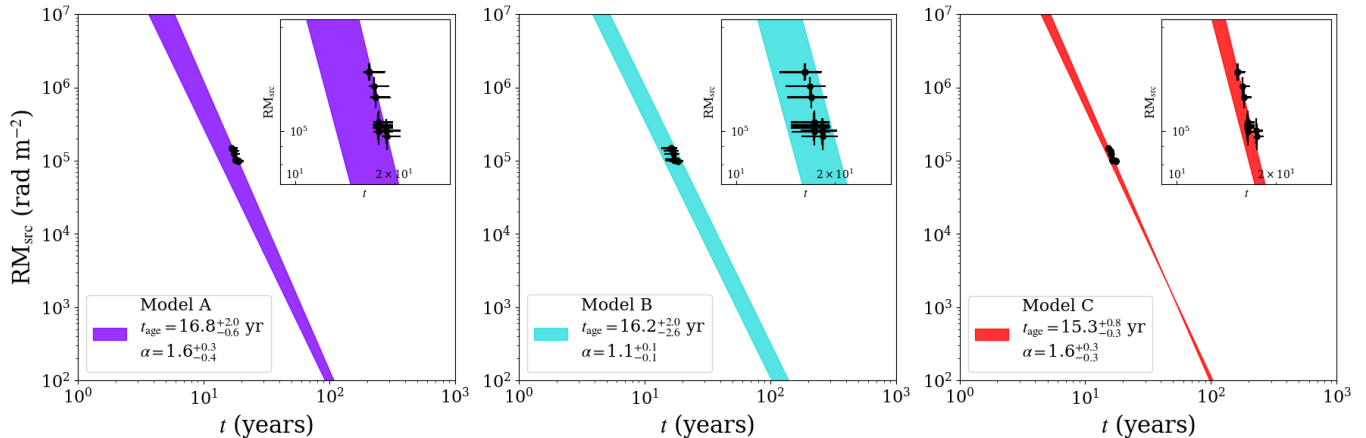


**Figure 6.** Source frame RM as a function of time for each model in [Margalit & Metzger \(2018\)](#). The ranges show the possible RMs from the parameters obtained in this work with 1-sigma uncertainties (Table 4). The black dots are the source frame RMs of FRB 121102, starting at the obtained  $t_{\text{age}}$  for each model. The RM uncertainties calculated from Eq. B3. The insets are zoomed in to the RM-time space around each  $t_{\text{age}}$ . *Left:* Model A. *Center:* Model B. *Right:* Model C.

## APPENDIX

### A. MODEL DESCRIPTIONS

#### A.1. *Piro & Gaensler (2018)*

[Piro & Gaensler \(2018\)](#) model the temporal evolution of both RM and DM of an expanding SNR. They consider three cases of evolutionary environments, which we expand upon below.

The first evolutionary case is an SNR that expands into an ISM of constant density. The shocked, ionized regions of the SN ejecta and ISM, as well as ionized material from the pulsar wind nebula close to the SNR center, provide sufficient free electrons to disperse an FRB. The Faraday rotation arises from the magnetic fields generated by the forward and reverse shocks during the SNR expansion. The SNR dominates both the DM and RM contributions at early times until the ISM takes over on a timescale of  $\sim 10^2 - 10^3$  years. The free parameters in this model are the number density of the uniform ISM,  $n$ , and the SN ejecta mass,  $M$ . The energy of the explosion is kept constant as  $E = 10^{51}$  erg for all cases.

The second case is where the stellar wind of the massive progenitor affects the circumstellar environment. The magnetized wind provides another source of magnetic field as well as altering the DM evolution. The DM is much higher initially compared to the previous scenario due to high density for the wind adjacent to the SN, but the DM decreases more rapidly because of the wind’s decreasing density. The wind environment can produce an ordered magnetic field, which is swept up by the SNR. This is the focal point of RM generation in

this scenario as opposed to the shock generation of magnetic fields in the previous scenario. The RM also drops rapidly due to the steep decline with time of the wind’s density and magnetic field. Here the free parameters are the ejecta mass,  $M$ , and the wind mass loading parameter,  $K$ , which is a function of the mass loss rate,  $\dot{M}$ , and wind velocity,  $v_w$ , and is given in units of  $\text{g cm}^{-1}$ .

The third is a mixture of the first two scenarios; an SNR expands into an ISM affected by a constant velocity wind, with  $M$  and  $K$  as free parameters. For all three cases they assume supernova ejecta masses of  $10 M_{\odot}$  (red supergiant progenitor) and  $2 M_{\odot}$  (stripped-envelope SN).

#### A.2. *Margalit & Metzger (2018)*

[Margalit & Metzger \(2018\)](#) consider a magnetar surrounded by a magnetar nebula. Flares and winds from the magnetar inject particles and magnetic energy into the nebula that is in turn responsible for the large observed RM. Their model is a one-zone magnetar nebula model, where they assume a spherical, freely expanding nebula with a constant radial velocity,  $v_n$ . The free magnetic energy of the magnetar,  $E_{B*}$  is released into the nebula at a rate following a power-law in time,  $\dot{E} \propto t^{-\alpha}$  ([Margalit & Metzger 2018](#), Eq. 4), where  $\alpha \gtrsim 1$ . The Faraday rotation occurs in non-relativistic electrons ejected earlier in the nebula’s history and cooled from radiation and adiabatic expansion.

In this model, the RM can be approximated as ([Margalit & Metzger 2018](#), Eq. 19, values normalised to 1

are omitted for clarity)

$$\begin{aligned} \text{RM}_5 \approx & 6 \left( \frac{E_{B_*}}{10^{50} \text{ erg}} \right)^{3/2} \left( \frac{v_n}{10^{17} \text{ cm/s}} \right)^{-7/2} \\ & \times (\alpha - 1)^{3/2} t_0^{(\alpha-1)/2} t^{-(6+\alpha)/2} \text{ rad m}^{-2}, \end{aligned} \quad (\text{A1})$$

where  $\text{RM}_5 \equiv \text{RM}/10^5 \text{ rad m}^{-2}$ ,  $E_{B_*}$  is in erg,  $v_n$  in  $\text{cm s}^{-1}$ ,  $t$  is seconds since the SN explosion, and  $t_0$  is the time in seconds since the onset of the active period of the magnetar’s energy release into the nebula. We obtain  $t_{\text{age}}$  from Eq. A1 by replacing  $t$  with  $t_{\text{age}} + t'$ , where  $t'$  is the time elapsed in seconds of each RM measurement since the first one.

For completeness, the estimated DM contribution from the Faraday-rotating medium is given by

$$\begin{aligned} \text{DM} \sim & 3 \times 10^{18} \left( \frac{E_{B_*}}{10^{50}} \right) \left( \frac{v_n}{10^8} \right)^{-2} \\ & \times (\alpha - 1) t^{-2} \text{ pc cm}^{-3} \end{aligned} \quad (\text{A2})$$

In their analysis, Margalit & Metzger (2018) consider three variations of their model with each having its own set of values for  $E_{B_*}$ ,  $t_0$ ,  $v_n$ , and  $\alpha$ . They call these variations ‘model A, B, and C’, and we keep the same notation to avoid confusion. Margalit & Metzger (2018) use models A, B, and C to estimate  $t_{\text{age}}$  of FRB 121102 from Eq. A1 using the RM measurements from Michilli et al. (2018a) and Gajjar et al. (2018). Their choice of parameters and their results are shown in Table 4.

## B. MODEL FITTING

To perform an MCMC we used the `emcee`<sup>12</sup> Python package (Foreman-Mackey et al. 2013). MCMC deploys random walkers around the initial estimates of the parameters, where the walkers explore the parameter space in order to reconstruct the posterior probability of the parameters.

To obtain an initial estimate for our parameters we used the `scipy` (Virtanen et al. 2020) stochastic least squares module `differential_evolution`. An initial guess is also required for `differential_evolution`, where we used the parameters of each model variety in Piro & Gaensler (2018) and Margalit & Metzger (2018). For our MCMC we randomly scattered 10 walkers around each parameter (up to 10% away), where each walker was made to walk  $1.5 \times 10^3$  steps. We used uninformative uniform priors for all our model parameters.

We introduced an error added in quadrature,  $\Sigma$ , to our observed RM uncertainties to be able to properly explore the free parameter space and to obtain more conservative uncertainties on our model parameters.  $\Sigma$  enters our Gaussian likelihood function as an underestimation factor of the variance  $\sigma$  (observed RM uncertainties in this case) as

$$s^2 = \sigma^2 + \Sigma^2. \quad (\text{B3})$$

The measured RM uncertainties,  $\sigma$ , are on the order of  $\lesssim 10^2 \text{ rad m}^{-2}$ .

The 2D posterior corner plots obtained from fitting the models of Piro & Gaensler (2018) and Margalit & Metzger (2018) to our data are shown in Figs. 7–8.

## REFERENCES

- Bannister, K. W., Deller, A. T., Phillips, C., et al. 2019, *Science*, doi: [10.1126/science.aaw5903](https://doi.org/10.1126/science.aaw5903)
- Bassa, C. G., Tendulkar, S. P., Adams, E. A. K., et al. 2017, *ApJL*, 843, L8, doi: [10.3847/2041-8213/aa7a0c](https://doi.org/10.3847/2041-8213/aa7a0c)
- Beloborodov, A. M. 2017, *ApJL*, 843, L26, doi: [10.3847/2041-8213/aa78f3](https://doi.org/10.3847/2041-8213/aa78f3)
- . 2019, arXiv e-prints, arXiv:1908.07743. <https://arxiv.org/abs/1908.07743>
- Brentjens, M. A., & de Bruyn, A. G. 2005, *A&A*, 441, 1217, doi: [10.1051/0004-6361:20052990](https://doi.org/10.1051/0004-6361:20052990)
- Burn, B. J. 1966, *MNRAS*, 133, 67, doi: [10.1093/mnras/133.1.67](https://doi.org/10.1093/mnras/133.1.67)
- Caleb, M., Stappers, B. W., Abbott, T. D., et al. 2020, *MNRAS*, 496, 4565, doi: [10.1093/mnras/staa1791](https://doi.org/10.1093/mnras/staa1791)
- Chatterjee, S., Law, C. J., Wharton, R. S., et al. 2017, *Nature*, 541, 58, doi: [10.1038/nature20797](https://doi.org/10.1038/nature20797)
- Chawla, P., Andersen, B. C., Bhardwaj, M., et al. 2020, *ApJL*, 896, L41, doi: [10.3847/2041-8213/ab96bf](https://doi.org/10.3847/2041-8213/ab96bf)
- CHIME/FRB Collaboration, Amiri, M., Bandura, K., et al. 2019a, *Nature*, 566, 235, doi: [10.1038/s41586-018-0864-x](https://doi.org/10.1038/s41586-018-0864-x)
- CHIME/FRB Collaboration, Andersen, B. C., Bandura, K., et al. 2019b, *ApJL*, 885, L24, doi: [10.3847/2041-8213/ab4a80](https://doi.org/10.3847/2041-8213/ab4a80)
- Chime/Frb Collaboration, Amiri, M., Andersen, B. C., et al. 2020, *Nature*, 582, 351, doi: [10.1038/s41586-020-2398-2](https://doi.org/10.1038/s41586-020-2398-2)
- Cruces, M., Spitler, L. G., Scholz, P., et al. 2020, arXiv e-prints, arXiv:2008.03461. <https://arxiv.org/abs/2008.03461>
- Desvignes, G., Eatough, R. P., Pen, U. L., et al. 2018, *ApJL*, 852, L12, doi: [10.3847/2041-8213/aaa2f8](https://doi.org/10.3847/2041-8213/aaa2f8)

<sup>12</sup> [emcee.readthedocs.io](https://emcee.readthedocs.io)

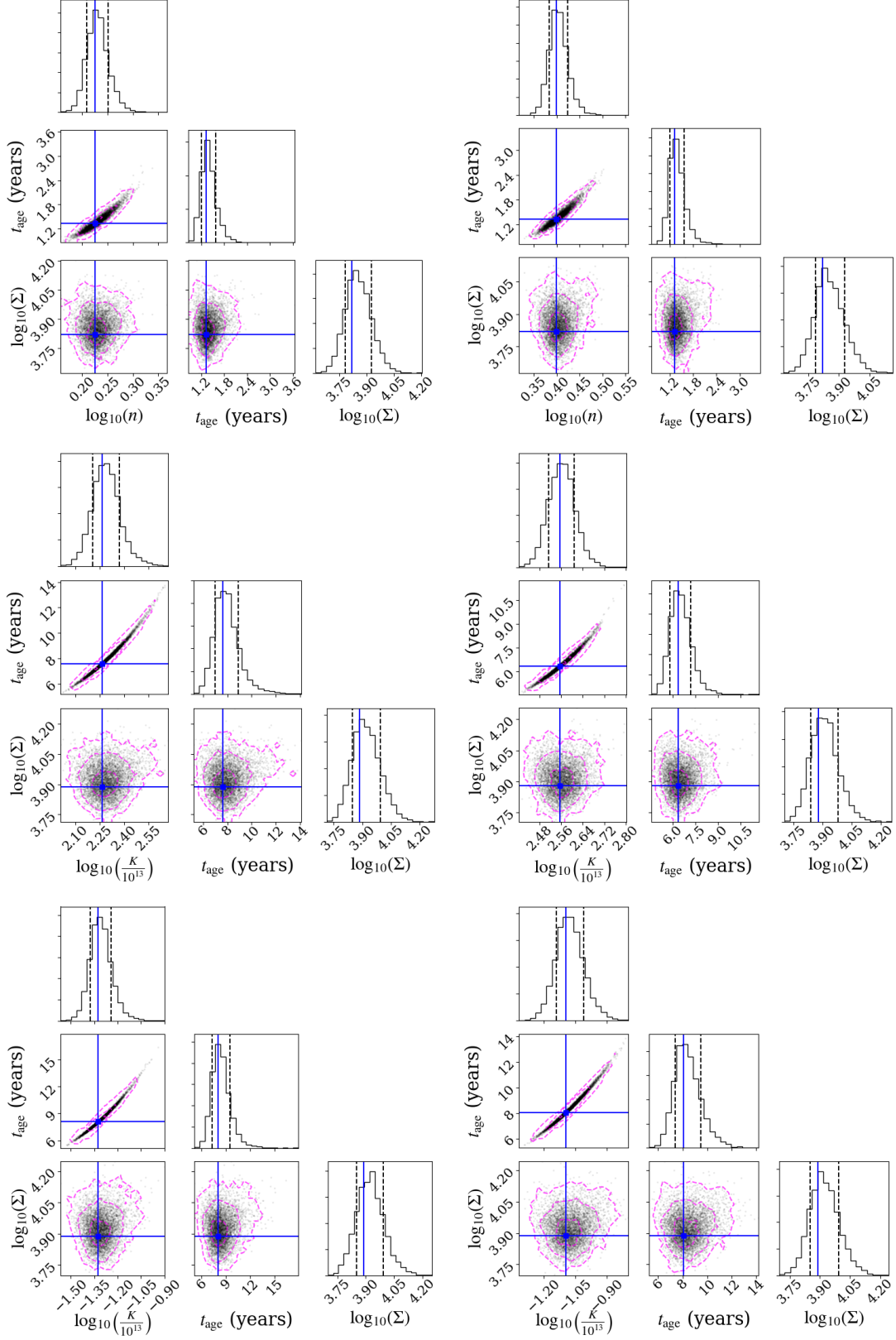


**Figure 7.** 2D posterior corner plot for the parameters  $(n, K, t_{\text{age}}, \text{and } \Sigma)$  of the models in Piro & Gaensler (2018). The histograms indicate the posterior probability of each parameter, with the dashed vertical lines denoting the 1-sigma range. The plots show the explored parameter space, with 1, 2, and 3 sigma dashed contours. The crosses indicate the prior used for each parameter, obtained with a stochastic least squares method. The left column shows the results for a  $10 M_{\odot}$  ejecta, and the right column for a  $2 M_{\odot}$  ejecta. *Top row:* Uniform ISM model. *Middle row:* Progenitor wind model. *Bottom row:* Progenitor wind and evolving supernova remnant model.

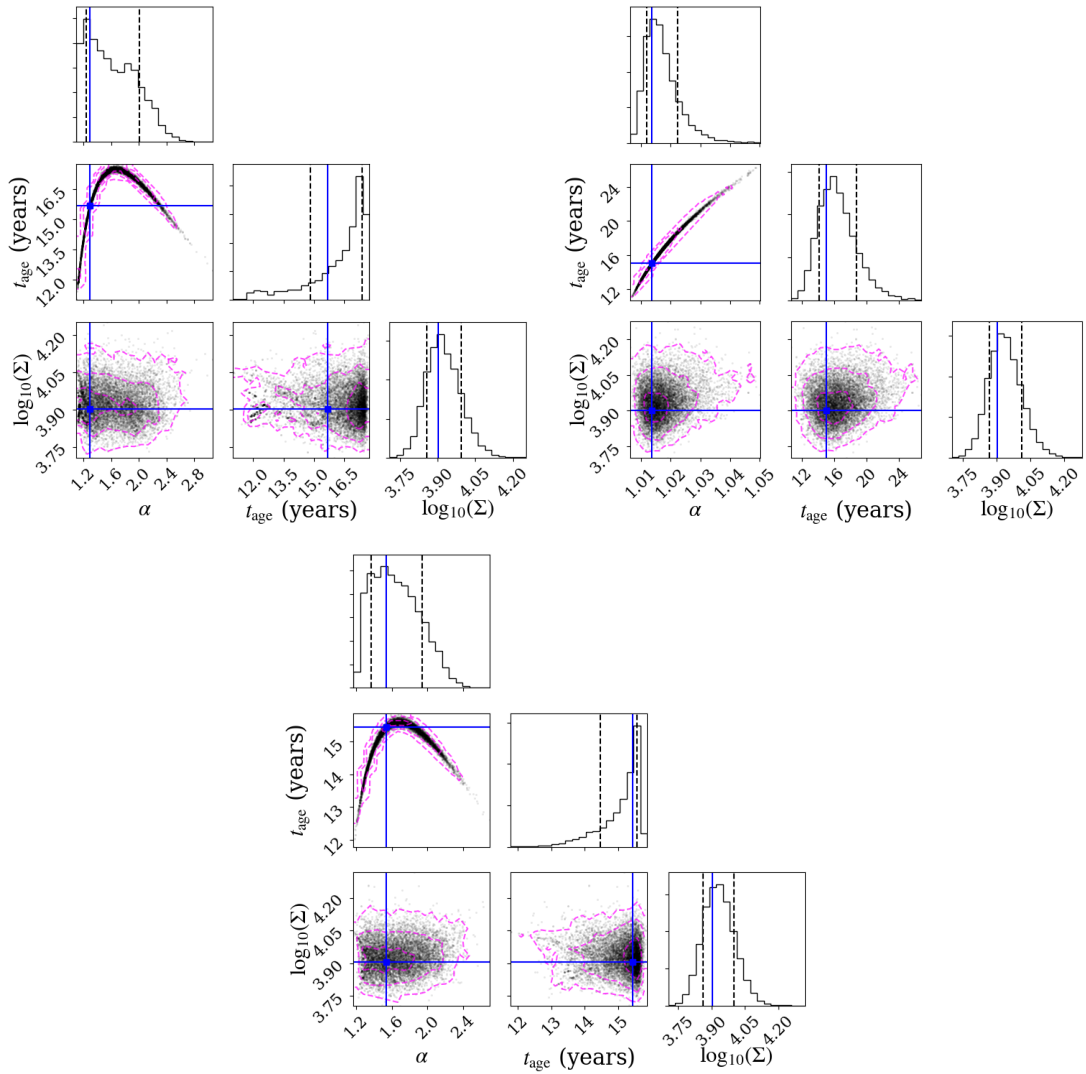


**Figure 8.** 2D posterior corner plot for the parameters ( $\alpha$ ,  $t_{\text{age}}$ , and  $\Sigma$ ) of the models in Margalit & Metzger (2018). The histograms indicate the posterior probability of each parameter, with the dashed vertical lines denoting the 1-sigma range. The plots show the explored parameter space, with 1, 2, and 3 sigma dashed contours. The crosses indicate the prior used for each parameter, obtained with a stochastic least squares method. *Top left:* Model A. *Top right:* Model B. *Bottom:* Model C.



- Eatough, R. P., Falcke, H., Karuppusamy, R., et al. 2013, *Nature*, 501, 391, doi: [10.1038/nature12499](https://doi.org/10.1038/nature12499)
- Fonseca, E., Andersen, B. C., Bhardwaj, M., et al. 2020, arXiv e-prints, arXiv:2001.03595. <https://arxiv.org/abs/2001.03595>
- Foreman-Mackey, D., Hogg, D. W., Lang, D., & Goodman, J. 2013, *PASP*, 125, 306, doi: [10.1086/670067](https://doi.org/10.1086/670067)
- Gajjar, V., Siemion, A. P. V., Price, D. C., et al. 2018, *ApJ*, 863, 2, doi: [10.3847/1538-4357/aad005](https://doi.org/10.3847/1538-4357/aad005)
- Gruzinov, A., & Levin, Y. 2019, *ApJ*, 876, 74, doi: [10.3847/1538-4357/ab0fa3](https://doi.org/10.3847/1538-4357/ab0fa3)
- Hamilton, P. A., Hall, P. J., & Costa, M. E. 1985, *MNRAS*, 214, 5P, doi: [10.1093/mnras/214.1.5P](https://doi.org/10.1093/mnras/214.1.5P)
- Heald, G. 2009, in *IAU Symposium*, Vol. 259, *Cosmic Magnetic Fields: From Planets, to Stars and Galaxies*, ed. K. G. Strassmeier, A. G. Kosovichev, & J. E. Beckman, 591–602, doi: [10.1017/S1743921309031421](https://doi.org/10.1017/S1743921309031421)
- Hessels, J. W. T., Spitler, L. G., Seymour, A. D., et al. 2019, *ApJL*, 876, L23, doi: [10.3847/2041-8213/ab13ae](https://doi.org/10.3847/2041-8213/ab13ae)
- Hilmarsson, G. H., Spitler, L. G., Keane, E. F., et al. 2020, *MNRAS*, 493, 5170, doi: [10.1093/mnras/staa701](https://doi.org/10.1093/mnras/staa701)
- Hotan, A. W., van Straten, W., & Manchester, R. N. 2004, *PASA*, 21, 302, doi: [10.1071/AS04022](https://doi.org/10.1071/AS04022)
- Johnston, S., Hobbs, G., Vigeland, S., et al. 2005, *MNRAS*, 364, 1397, doi: [10.1111/j.1365-2966.2005.09669.x](https://doi.org/10.1111/j.1365-2966.2005.09669.x)
- Josephy, A., Chawla, P., Fonseca, E., et al. 2019, *ApJL*, 882, L18, doi: [10.3847/2041-8213/ab2c00](https://doi.org/10.3847/2041-8213/ab2c00)
- Kumar, P., Shannon, R. M., Osłowski, S., et al. 2019, *ApJL*, 887, L30, doi: [10.3847/2041-8213/ab5b08](https://doi.org/10.3847/2041-8213/ab5b08)
- Lyubarsky, Y. 2014, *MNRAS*, 442, L9, doi: [10.1093/mnrasl/slu046](https://doi.org/10.1093/mnrasl/slu046)
- Macquart, J. P., Prochaska, J. X., McQuinn, M., et al. 2020, *Nature*, 581, 391, doi: [10.1038/s41586-020-2300-2](https://doi.org/10.1038/s41586-020-2300-2)
- Marcote, B., Paragi, Z., Hessels, J. W. T., et al. 2017, *ApJL*, 834, L8, doi: [10.3847/2041-8213/834/2/L8](https://doi.org/10.3847/2041-8213/834/2/L8)
- Marcote, B., Nimmo, K., Hessels, J. W. T., et al. 2020, *Nature*, 577, 190, doi: [10.1038/s41586-019-1866-z](https://doi.org/10.1038/s41586-019-1866-z)
- Margalit, B., & Metzger, B. D. 2018, *ApJL*, 868, L4, doi: [10.3847/2041-8213/aaedad](https://doi.org/10.3847/2041-8213/aaedad)
- Metzger, B. D., Berger, E., & Margalit, B. 2017, *ApJ*, 841, 14, doi: [10.3847/1538-4357/aa633d](https://doi.org/10.3847/1538-4357/aa633d)
- Metzger, B. D., Margalit, B., & Sironi, L. 2019, *MNRAS*, 485, 4091, doi: [10.1093/mnras/stz700](https://doi.org/10.1093/mnras/stz700)
- Michilli, D., & Hessels, J. W. T. 2018, *SpS: Single-pulse Searcher*. <http://ascl.net/1806.013>
- Michilli, D., Seymour, A., Hessels, J. W. T., et al. 2018a, *Nature*, 553, 182, doi: [10.1038/nature25149](https://doi.org/10.1038/nature25149)
- Michilli, D., Hessels, J. W. T., Lyon, R. J., et al. 2018b, *MNRAS*, 480, 3457, doi: [10.1093/mnras/sty2072](https://doi.org/10.1093/mnras/sty2072)
- Oppermann, N., Yu, H.-R., & Pen, U.-L. 2018, *MNRAS*, 475, 5109, doi: [10.1093/mnras/sty004](https://doi.org/10.1093/mnras/sty004)
- Petroff, E., Hessels, J. W. T., & Lorimer, D. R. 2019, *A&A Rv*, 27, 4, doi: [10.1007/s00159-019-0116-6](https://doi.org/10.1007/s00159-019-0116-6)
- Petroff, E., Barr, E. D., Jameson, A., et al. 2016, *PASA*, 33, e045, doi: [10.1017/pasa.2016.35](https://doi.org/10.1017/pasa.2016.35)
- Piro, A. L. 2016, *ApJ*, 824, L32, doi: [10.3847/2041-8205/824/2/L32](https://doi.org/10.3847/2041-8205/824/2/L32)
- Piro, A. L., & Gaensler, B. M. 2018, *ApJ*, 861, 150, doi: [10.3847/1538-4357/aac9bc](https://doi.org/10.3847/1538-4357/aac9bc)
- Prochaska, J. X., Macquart, J.-P., McQuinn, M., et al. 2019, *Science*, 366, 231, doi: [10.1126/science.aay0073](https://doi.org/10.1126/science.aay0073)
- Rajwade, K. M., Mickaliger, M. B., Stappers, B. W., et al. 2020, arXiv e-prints, arXiv:2003.03596. <https://arxiv.org/abs/2003.03596>
- Ransom, S. 2011, *PRESTO: Pulsar Exploration and Search TOolkit*. <http://ascl.net/1107.017>
- Ravi, V., Catha, M., D’Addario, L., et al. 2019, *Nature*, 572, 352, doi: [10.1038/s41586-019-1389-7](https://doi.org/10.1038/s41586-019-1389-7)
- Reines, A. E., Condon, J. J., Darling, J., & Greene, J. E. 2020, *ApJ*, 888, 36, doi: [10.3847/1538-4357/ab4999](https://doi.org/10.3847/1538-4357/ab4999)
- Seymour, A., Michilli, D., & Pleunis, Z. 2019, *DM-phase: Algorithm for correcting dispersion of radio signals*. <http://ascl.net/1910.004>
- Spitler, L. G., Cordes, J. M., Chatterjee, S., & Stone, J. 2012, *ApJ*, 748, 73, doi: [10.1088/0004-637X/748/2/73](https://doi.org/10.1088/0004-637X/748/2/73)
- Spitler, L. G., Cordes, J. M., Hessels, J. W. T., et al. 2014, *ApJ*, 790, 101, doi: [10.1088/0004-637X/790/2/101](https://doi.org/10.1088/0004-637X/790/2/101)
- Spitler, L. G., Scholz, P., Hessels, J. W. T., et al. 2016, *Nature*, 531, 202, doi: [10.1038/nature17168](https://doi.org/10.1038/nature17168)
- Spitler, L. G., Herrmann, W., Bower, G. C., et al. 2018, *ApJ*, 863, 150, doi: [10.3847/1538-4357/aad332](https://doi.org/10.3847/1538-4357/aad332)
- Tendulkar, S. P., Bassa, C. G., Cordes, J. M., et al. 2017, *ApJL*, 834, L7, doi: [10.3847/2041-8213/834/2/L7](https://doi.org/10.3847/2041-8213/834/2/L7)
- The CHIME/FRB Collaboration, Amiri, M., Andersen, B. C., et al. 2020, arXiv e-prints, arXiv:2001.10275. <https://arxiv.org/abs/2001.10275>
- van Straten, W., & Bailes, M. 2011, *PASA*, 28, 1, doi: [10.1071/AS10021](https://doi.org/10.1071/AS10021)
- Vedantham, H. K., & Ravi, V. 2019, *MNRAS*, 485, L78, doi: [10.1093/mnrasl/slz038](https://doi.org/10.1093/mnrasl/slz038)
- Virtanen, P., Gommers, R., Oliphant, T. E., et al. 2020, *Nature Methods*, 17, 261, doi: <https://doi.org/10.1038/s41592-019-0686-2>
- Zhang, B. 2018, *ApJL*, 854, L21, doi: [10.3847/2041-8213/aaadba](https://doi.org/10.3847/2041-8213/aaadba)
- Zhang, Y. G., Gajjar, V., Foster, G., et al. 2018, *ApJ*, 866, 149, doi: [10.3847/1538-4357/aadf31](https://doi.org/10.3847/1538-4357/aadf31)